This work was carried out in whole or in part within the framework of the NOMATEN Center of Excellence, supported from the European Union Horizon 2020 research and innovation programme (Grant Agreement No. 857470) and from the European Regional Development Fund via the Foundation for Polish Science International Research Agenda PLUS programme (Grant No. MAB PLUS/2018/8).

This is a copy of the publication which appeared in: Materials Science & Engineering A vol 846 (2022) 143270, published on: 13 May 2022.

DOI: 10.1016/j.msea.2022.143270

Materials Science & Engineering A 846 (2022) 143270

Contents lists available at ScienceDirect

Materials Science & Engineering A

journal homepage: www.elsevier.com/locate/msea

Effects of surface curvature and dislocation dynamics: Dynamical deformation mechanisms for uniaxial compression tests at the nanoscale

Fabrizio Rovaris [a,*], Stefanos Papanikolaou [a], Mikko J. Alava [a,b]

[a] NOMATEN Centre of Excellence. National Centre for Nuclear Research, Ul. A. Soltana 7 05-400 Swierk Otwock, Poland
[b] Department of Applied Physics, Aalto University, P.O. Box 11000 00076 Aalto Espoo, Finland

ARTICLE INFO

Keywords:
Plasticity
Dislocation dynamics
Finite element modeling

ABSTRACT

The understanding of size effects in micro-crystal plasticity has been in-part based on controlled uniaxial mechanical testing of crystalline micropillars that may be monitored in-situ, using modern microscopy approaches. Nevertheless, it has always been clear that mechanics and materials science are not ideally decoupled in uniaxial micropillar compression, thus agreement between experiments and theory remains challenging. We present a theoretical analysis of the uniaxial compression of micropillars with curved top free surfaces, in consistency with modern experimental thresholds. By using coupled Finite Element and Discrete Dislocation Dynamics simulations we investigate the effect of the small curvature to dislocation microstructure evolution at constant displacement rate. The uniaxial compression of flat micropillars is shown to be consistent with existing literature, with homogeneous stress build up and random activation of sources inside the volume. However, in the presence of a small top-surface micropillar curvature, there are significant dynamical effects on dislocation mechanisms and an overestimate of strain at yielding that leads to large errors on capturing elastic compression moduli and avalanche noise characteristics. Characteristically, for 10 nm-high isotropic curvature, large (> 100 MPa) stress drops emerge in the average stress, that become *larger* as the initial dislocation density increases, in direct contrast to expectations and findings for ideally flat micropillars.

1. Introduction

Mechanical properties of materials at the microscale differ substantially from bulk ones, and the incorporation of size effects is crucial for deeper physical understanding [1–3]. A key tool for the investigation of such microscale size effects emerged with the advance of microscale testing through the combination of flat-punch nanoindentation and Focused Ion Beam (FIB) [4–6]: these experiments are typically conducted by using FIB to cut a micron-sized pillar out of a bulk material surface, and then compress it with a flat indenter. The advantage of this test has been the nearly uniaxial compression condition, that allows the decoupling of materials science and mechanics, with a nearly homogeneous stress field across the sample. This aspect greatly simplifies the analysis and interpretation of recorded data [7–9]. Recent findings in this field revealed that the flow stress (s) of metallic micropillars correlates with the pillar radius (R) for a wide variety of metals [10–14]. Commonly accepted explanations for the increase of the flow stress at a smaller scale include the dislocation starvation (DS) model and the single arm source (SAS) model [2,15–18]. However, the nearly uniaxial compression condition for microscale pillars is not ideal, and the importance of the relative deviation is dependent on the pillar's dislocation ensemble. In this Paper we consider the effect of an isotropically curved top pillar surface in order to investigate the effect of pillar's initial dislocation configurations into the dynamical dislocation mechanisms and observed size effects. We find that there is a significant stress inhomogeneity and an increase of the avalanche noise with *increasing* dislocation density, in direct contrast with findings for the ideally flat micropillars.

Recently, Transmission Electron Microscopy (TEM) experiments [19–21] have been utilized to elucidate dislocation dynamics during uniaxial pillar compression [10,22]. TEM techniques consist in performing mechanical testing inside the chamber of a TEM allowing for the collection of stress/strain curves and TEM imaging aligned in time. This provides a rich set of data, with direct insights into the dislocation dynamics in the specimen during compression. In this way, dislocation activity can be directly observed and correlated to features of the stress/strain curve, allowing for the interpretation of complex systems that would be otherwise impossible, like the plasticity behavior of High Entropy Alloys (HEAs) [23–25]. However, in this Paper, we show that dynamical dislocation mechanisms that emerge in uniaxial pillar compression experiments may be an outcome of a distorted geometry

* Corresponding author.
E-mail address: fabrizio.rovaris@ncbj.gov.pl (F. Rovaris).

https://doi.org/10.1016/j.msea.2022.143270
Received 14 December 2021; Received in revised form 5 May 2022; Accepted 6 May 2022
Available online 13 May 2022

and thus, not reflect intrinsic HEA-specific mechanisms, that should relate directly to the chemical disorder in the microstructure.

The mechanics issues in micropillar compression experiments were noticed early on, thus shedding light on the importance of a proper experimental design [26,27]. Indeed, the quality of the recorded data is strongly dependent on the fabrication process and the experimental setup, especially because external defects (surface inhomogeneities, indenter/pillar misalignment,...) may severely alter results, in a way that does not represent the materials science, but instead is a mixed outcome of surface mechanics and intrinsic microstructural dynamics. In particular, all pillar surfaces, as well as the nanoindentation tip surface, are susceptible to precision and misalignment issues. A small surface roughness or a curvature on the top surface, may produce large stress inhomogeneities and thus alter the observed mechanical properties. There are several ways in mechanics to introduce stress inhomogeneities through misalignment issues in uniaxial pillar compression, with the most common being an angular misalignment of tip and top surfaces [3]. However, in this Paper, we are dedicated to understand how dislocation dynamics and mechanisms are altered due to such stress inhomogeneities, and quantify the severity of the issues for basic phenomenological conclusions in the field of uniaxial pillar compression, especially with respect to strengthening and avalanche effects in single crystalline metals [10].

In order to address the entity of this problem, we investigate here the effect of a small curvature on the free surface of micro-scale pillars on the evolution of the dislocation microstructures. For this purpose, we exploit Discrete Dislocation Dynamics (DDD) simulations [28]. DDD approaches [29] are able to simulate the behavior of individual dislocations at the mesoscale, a scale comparable to typical laboratory-scale testing, linking mechanical properties of a material to features of dislocation microstructures and their dynamics [30,31]. In this work, we develop a novel framework, by handling the possibility of dealing with arbitrary free-surface geometries, without approximate approaches to deal with the image contributions to dislocation stress fields. We present and apply a DDD approach that uses a Finite Element (FE) solver for arbitrary free surfaces, used to deal with the mechanical equilibrium problem set in term of a Partial Differential Equations (PDE) [32]. By exploiting this DDD approach, we perform simulations showing the evolution of dislocation microstructures in both flat and isotropically curved pillars in order to directly investigate the effect of a non-flat free surface on micropillar uniaxial compression.

The organization of the Paper is as follows. In Section 2, the numerical setup, and relevant simulation details are discussed. In Section 3, we demonstrate how the mechanical response of pillars is influenced by a small curvature on the top surface, that may introduce a bump of height less than a few nanometers, and that is in isotropic contact with a perfectly horizontally flat loading tip. In the same section, We discuss the connection of these results to basic phenomenological expectations for strengthening and size effects in uniaxial pillar compression of single crystalline metals. Finally, in Section 4, we present our conclusions, and discuss future research directions.

2. Methods: Dislocation dynamics simulations

The approach exploited in this paper to simulate the uniaxial compression of micropillars consists in a coupling between a three-dimensional (3D) DDD model (Ref. [33]) and a FE solver [34]. The coupling is based on the eigenstrain formalism [32,35], and implemented following the Discrete–Continuous Model (DCM) scheme [36–38]. In DDD, dislocations are discretized into small straight segments whose dynamics is dictated by the Peach–Koehler force:

$$F = (\boldsymbol{\sigma} \cdot \boldsymbol{b}) \times \boldsymbol{\xi} \tag{1}$$

where $\boldsymbol{\sigma}$ is the stress field acting at the position of the considered dislocation segment, $\boldsymbol{b}$ its Burgers vector and $\boldsymbol{\xi}$ the dislocation line direction.

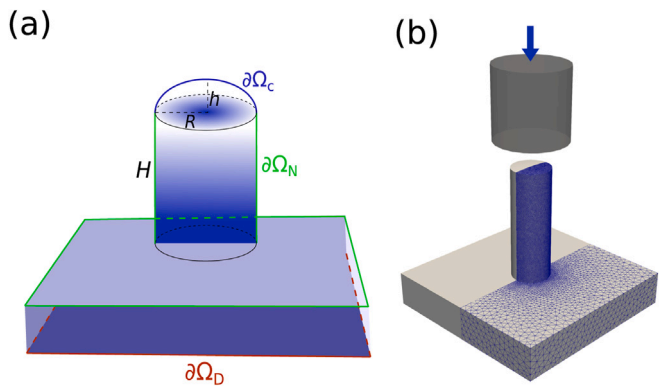

Fig. 1. (Color online) Schematic representation of FE model used to simulate the uniaxial compression of micropillars. (a) Sketch of the simulation geometry. The colored edges highlight the different boundary conditions applied for the FE model. (b) A rigid virtual indenter (in dark gray in the figure) is used to impose a displacement on the top surface of the pillar. A locally-refined mesh (colored in blue for half of the pillar) is used to efficiently evaluate the FE solution of the mechanical problem.

Once the local forces applied to each segment have been evaluated, their dynamics is simply evaluated in the assumption of free-flight dislocation motion, i.e. at temperature high enough for neglecting activated processes in dislocation motion. In this regime the velocity v of a straight segment is directly proportional to the resolved shear stress on its glide plane τ_a:

$$v = \frac{\tau_a b}{B} \tag{2}$$

with B the viscous drag coefficient.

In the DCM, the plastic deformation produced by the movement of each single dislocation segment is spread over a finite volume by means of a suitable distribution function with a characteristic thickness $\tilde{h}$. In this way, the eigenstrain formalism can be properly implemented using FE. More specifically, the distribution function used is the one proposed in Ref. [39] to develop a non-singular theory of dislocations. Thus, in the DCM approach, the local stress field $\boldsymbol{\sigma}$ in Eq. (1) can be evaluated by solving the problem of mechanical equilibrium set in terms of a Partial Differential (PD) equation linking the unknown displacement field $\boldsymbol{u}$, to a generic applied deformation eigenstrain ϵ^*:

$$\begin{cases} -\nabla\vec{\sigma}(\vec{u}) = \vec{0} & \text{on } \Omega \setminus \partial\Omega \\ \vec{\sigma}(\vec{u}) = C(\vec{\epsilon}(\vec{u}) - \vec{\epsilon}^*) & \text{on } \Omega \setminus \partial\Omega \\ \vec{u} = \vec{0} & \text{on } \partial\Omega_D \\ \vec{\sigma} \cdot \vec{n} = \vec{0} & \text{on } \partial\Omega_N \\ \vec{\sigma} \cdot \vec{n} - k_{pen}\langle u - Z\rangle_+ = \vec{0} & \text{on } \partial\Omega_c \end{cases} \tag{3}$$

where Ω is the simulation volume and $\partial\Omega$ its external boundary. The bottom boundary $\partial\Omega_D$ is kept fixed by applying Dirichlet boundary conditions (zero displacement), while $\partial\Omega_N$ is the top free surface with Neumann boundary conditions (zero normal stress). The last condition in Eq. (3), is applied to the contact region $\partial\Omega_c$. The boundary conditions here defined correspond to the colored regions in Fig. 1(a). The constant k_{pen} is a penalization constant and the symbol $\langle\rangle_+$ denotes the positive part of the argument. The function Z is used to virtually define the indenter location. In the present work, we focus on the contact between a micropillar and a flat indenter and thus Z reduces to a constant value, but it can be easily generalized to an arbitrary indenter tip shape. When rewriting this PDE in the weak form this last penalty condition become:

$$\int \sigma(u) : \epsilon(v)\,\mathrm{d}\Omega + k_{pen}\int_{\partial\Omega_{top}} \langle u - Z\rangle_+ v\,\mathrm{d}S = 0 \tag{4}$$

where v is the test function.

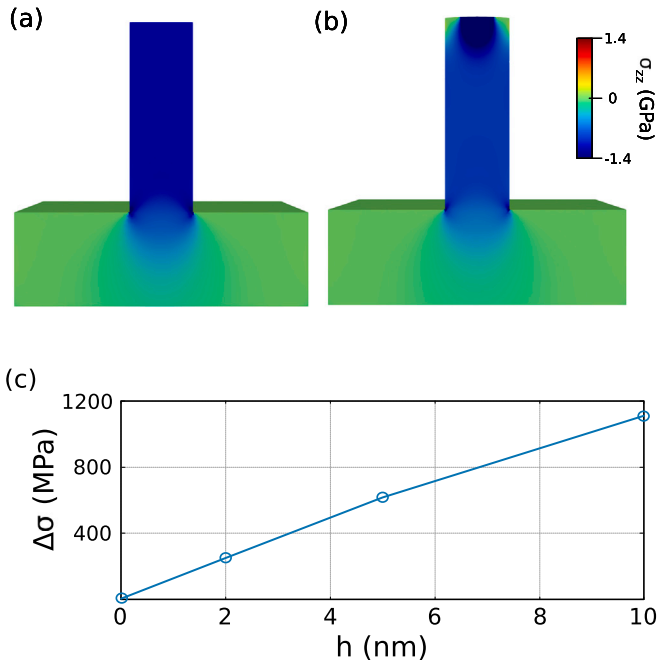

Fig. 2. (Color online) Stress maps (σ_{zz} component) showing the resulting stress field after a 1% compression of a, respectively, flat pillar (a) and a pillar with a curvature corresponding to $h = 10$ nm (b). (c) Plot of the stress difference (top vs center of the pillar) as function of h.

The PD problem defined in Eq. (3) is generally formulated for describing the response of a system to an applied deformation ϵ^*. This generalization can be used to describe the plastic deformation induced by the movement of dislocations exploiting the eigenstrain formalism, originally formulated by Elsheby to describe inclusions in solids [40], discussed in Ref. [35] and originally implemented in DDD in Ref. [32]. The elementary plastic deformation $d\vec{\epsilon}_p$ produced by the motion of dislocation segment is regularized by a distribution function $\tilde{w}$:

$$\mathrm{d}\vec{\epsilon}_p = \tilde{w}(r,\tilde{h})\frac{\vec{b}\otimes\mathrm{d}\vec{A}+\mathrm{d}\vec{A}\otimes\vec{b}}{2} \tag{5}$$

where $\mathrm{d}\vec{A}$ is the (oriented) area swept by the dislocation segment during its motion and $\tilde{h}$ is a characteristic thickness for the regularization function $\tilde{w}$. The homogenization function $\tilde{w}$ is a truncated expression of the w^{C} function introduced by Cai et al. in Ref. [39]:

$$\begin{aligned} w(r,\tilde{h}) &= \frac{15h^4}{8\pi(r^2+\tilde{h}^2)^{7/2}} \\ w^{\mathrm{C}}(r,\tilde{h}) &= 0.3425w(r,0.9038\tilde{h}) + 0.6575w(r,0.5451\tilde{h}) \end{aligned} \tag{6}$$

with the truncation defined by:

$$\tilde{w}(r,\tilde{h}) = \mathcal{H}(r_c - r)w^{\mathrm{C}}(r,\tilde{h}) \tag{7}$$

and $\mathcal{H}$ the Heavyside function with the cutoff radius $r_c = 1.75\tilde{h}$ as discussed in Ref. [36] .

By integration of the $\mathrm{d}\vec{\epsilon}_p$ term over all the swept area $\mathrm{d}A$ and by summing this contributions for all the moving dislocation segments at a given time-step t of the simulation, we obtain the applied plastic deformation for the whole dislocation microstructure, $\vec{\epsilon}_p$. Then, this term is applied as an eigenstrain term in Eq. (3) and the stress field can be recovered by solving the elastic problem, using the FE method. In this way, boundary conditions for free surfaces of arbitrary geometry are fully taken into account when solving the PD system of Eqs. (3). Finally, the stress field resulting from the FE solution is plugged into Eq. (1) and is then used to compute forces that move dislocations at the $Nth+1$ time step, following an iterative process [32].

It is important to highlight that, while the FE solver is in charge of computing mechanical equilibrium, the dislocation dynamics code not only handles the movement of dislocation segments but it also manages potential reactions between them, modeling local interactions and recombinations. When two dislocation segments fall inside the regularized region their interaction is evaluated by means of the analytical expression derived in Ref. [39], consistently exploiting the same regularization function $\tilde{w}$. Thus, the dynamics described by the DCM model is independent on the choice of the regularization thickness $\tilde{h}$ [36].

For the simulations performed in this Paper, dipolar dislocation loops are placed randomly inside a copper single crystalline micropillar with a given initial dislocation density ρ [41]. The simulation geometry is schematically depicted in Fig. 1(a). A pillar with radius $R = 250$ nm and height $H = 1500$ nm is subjected to uniaxial compression in the vertical direction by means of a flat indenter. A small curvature is added on the top free surface and described by its height h. It is worth mentioning that the uniaxial character of the mechanical loading conditions is maintained, allowing for a clear interpretation of results in the context of phenomenologically known size effects [4]. As shown in Fig. 1(b), a spatially-resolved FE mesh has been used, in order to perform computationally efficient simulations. The mesh is highly refined in the contact region, as well as inside the micropillar bulk, where dislocation activity takes place. A substrate with smaller resolution and box shape is placed under the micropillar with periodic boundary conditions applied at the lateral surfaces and Dirichlet boundary conditions at the bottom.

3. Results and discussion

In this Section we present the results obtained from DDD simulations of uniaxial micropillar compression of pillars with small isotropic curvatures on the top free surface and the comparison with the ideally-flat case.

In Fig. 2(a) and (b), we show the stress field resulting after a 1% elastic deformation for the case of, respectively, a flat pillar and a pillar with $h = 10$ nm. The stress field is nearly homogeneous in the flat pillar, as expected. However, the presence of an even small curvature on top of the pillar, as shown in Fig. 2(b), consisting of a 10 nm height over a pillar diameter of 500 nm, produced a drastic change in the stress profile. A region of high stress field just below the contact area between the indenter and the top pillar surface can be observed, while the stress field in the central part of the pillar is lowered with respect to the flat case. The same behavior can be appreciated by looking at the plot of Fig. 2(c). Here, the stress difference between the average stress value in the middle of the pillar and the maximum value on its top is plotted against the value of h. These $\Delta\sigma$ for the considered h values are substantial compared to the stress values at the center, reaching nearly 100% of the central stress value when h is bigger than 5 nm. As can be observed in the figure, the stress difference increase with increasing the value of h due to the localization of the stress field in the contact region. The limiting case of such a scenario would be a very high-curvature pillar (or a sharp tip) contacting with the indenter. In this case, all the stress field would be concentrated in the tip and correspondingly also all the plastic deformation would be limited there. This can be compared with the corner effect that arise when an indenter contact the edge of a pillar [26]. A high stress field concentrates near the edge and the plastic deformation start in that region.

The observation of the elastic response of such a system already points out to a drastic difference in the mechanical behavior of the curved pillar with respect to the flat one. This has been further analyzed by performing DDD simulations on both the cases discussed above.

Let us start by showing the results of the simulations performed for the uniaxial compression of a pillar with an initial dislocation density $\rho = 10^{14}$ m^{-2} for the dipolar loops. Selected snapshots taken from the simulations are shown in Fig. 3 for the case of a curved pillar with $h = 10$ nm, Fig. 3(a), and a pillar with flat top surface, Fig. 3(b).

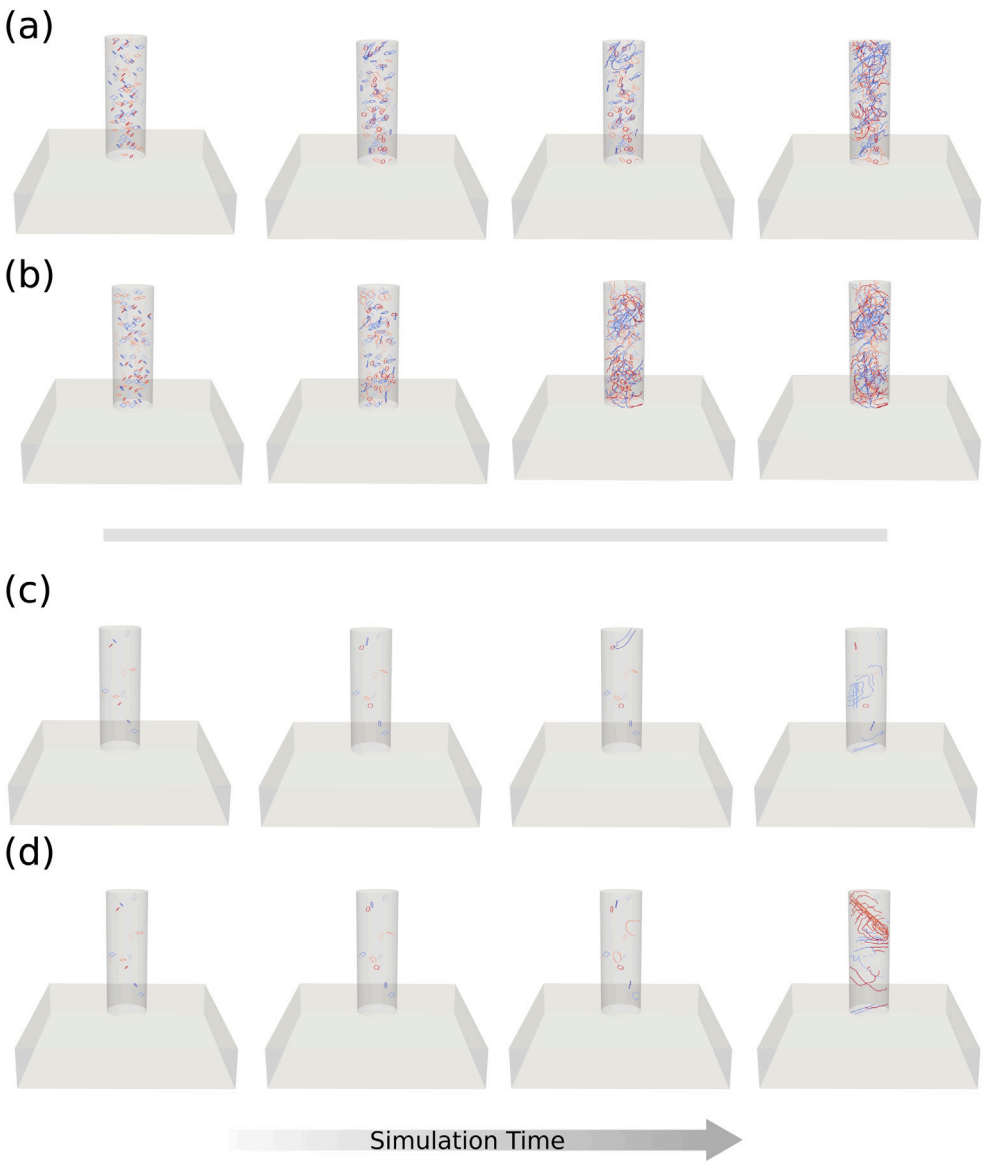

Fig. 3. (Color online) Selected snapshots of the evolution of a dislocation distribution during uniaxial compression for a pillar with initial dislocation density is $\rho = 10^{14}$ m^{-2} and a top surface with $h = 10$ nm (a) and a flat one (b). Both the simulations starts with exactly the same initial conditions. In (c) and (d) is reported again the evolution of the dislocation distribution for a pillar with initial dislocation density $\rho = 10^{13}$ m^{-2} and, respectively, a top surface with $h = 10$ nm (c) and a flat one (d).

As can be seen from the simulation, the presence of a non-flat free surface produce a visible effect on the evolution of the dislocation microstructure. In the top row of Fig. 3(a) it is possible to observe that the first dislocation loops activated lie just beyond the top free surface. In the corresponding stage for a flat pillar in the bottom row, Fig. 3(b), no dislocation activity is yet visible. This can be easily described in terms of the different stress field arising in the pillar and already shown in Fig. 2(a) and (b). For the case of the flat pillar, Fig. 2(a), the stress field produced at any given compression stage is nearly homogeneous and thus the onset for the activation of the dislocation motion and multiplication will be reached nearly simultaneously in the whole pillar. On the contrary, for the case of the curved pillar, Fig. 2(b), a highly-compressed region just below the top surface is present, confining the region of plastic activity in that region at the early stage of the deformation. At later stages, a more homogeneous stress field builds up in the pillars and randomly-positioned dislocation sources are activated, bot in the case of the curved flat free surface both in the case of the flat one. A similar scenario can be observed for the simulations performed a pillar with initial dislocation density of $\rho = 10^{13}$ m^{-2} and reported in Fig. 3(c)–(d) for, respectively, a curved pillar with $h = 10$ nm and a pillar with flat top surface. Here, the dislocation activities in the curved case is confined near the top free surface at the beginning of the deformation even if the lower statistics due to the low number of initial dislocation loops limit this effect to just one dislocation loop activated. At later stages the deformation behavior looks more similar for both the cases investigated. Furthermore, Fig. 4 shows the plastic activity for the simulations performed on a flat pillar with initial dislocation density $\rho = 10^{14}$ m^{-2}. The plastic strain evolution is shown as function of the simulation time. Again, the dislocation activity is nearly homogeneous for the case of a flat pillar, with dislocation sources randomly activated in the whole pillar volume. At the end of the simulation, shear bands can be observed, dispersed along he whole pillar height.

Key insights to the overall effects of the external surface curvature arise through the study of stress–strain curve fluctuations. Fig. 5 shows the stress–displacement curve for the case of the simulations with initial dislocation density $\rho = 10^{13}$ m^{-2} (a), $\rho = 10^{14}$ m^{-2} (b) and $\rho = 3 \times 10^{14}$ m^{-2} (c) for both the flat pillar and the pillar with $h = 10$ nm. A drastic difference in the stress/displacement curve can be observed. The pillar with a flat free surface shows as expected an

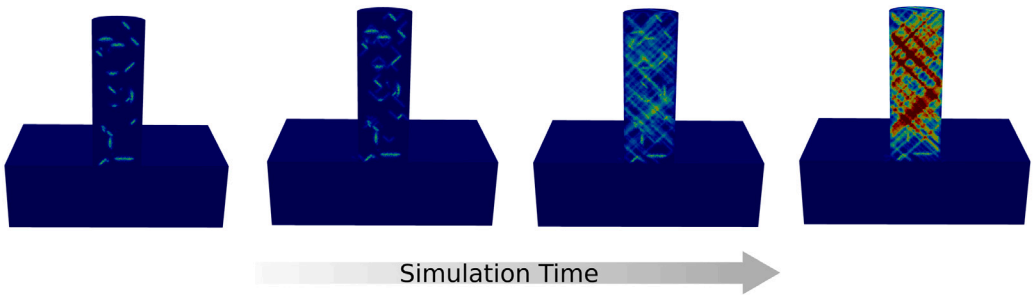

Fig. 4. (Color online) Selected snapshots of the plastic strain evolution during uniaxial compression for a pillar with a flat top surface. The initial dislocation density is $\rho = 10^{14}$ m^{-2}.

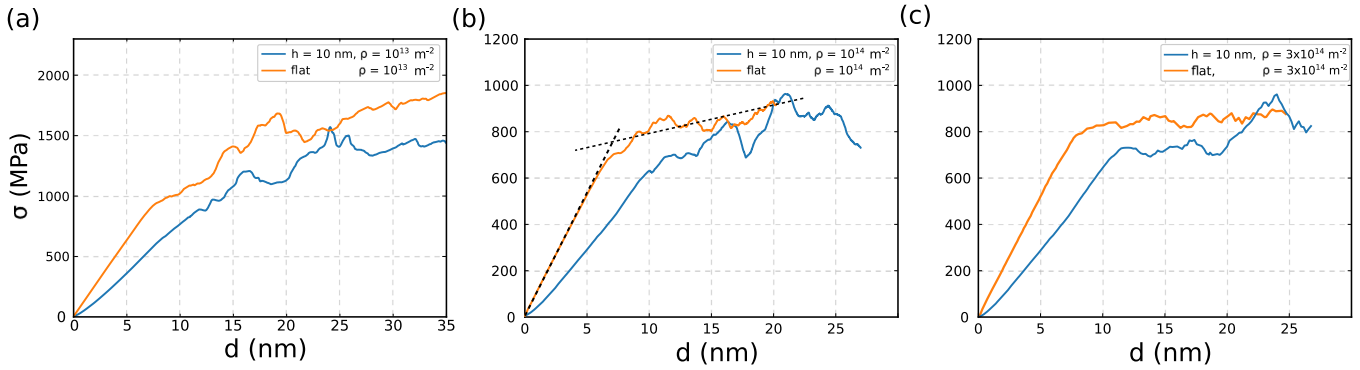

Fig. 5. (Color online) Stress–displacement curve obtained from the simulation of a flat pillar and a pillar with $h = 10$ nm and initial dislocation density $\rho = 10^{13}$ m^{-2} (a), $\rho = 10^{14}$ m^{-2} (b) and $\rho = 3 \times 10^{14}$ m^{-2} (c).

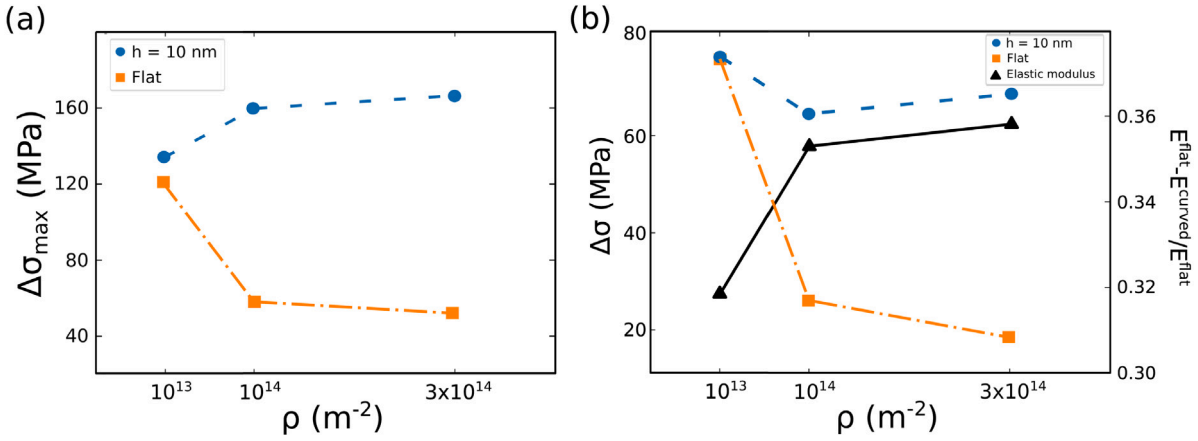

Fig. 6. (Color online) Maximum stress drops for all the simulations plotted against the initial dislocation density (a). Average stress drops, $\Delta\sigma$, and relative deviation in elastic constants plotted against the initial dislocation density (b).

initial linear response in the elastic regime up to the yielding point. On the other hand, the pillar with $h = 10$ nm shows a sub-linear response in the elastic regime that is not totally recovered at the yielding point. A corresponding strain at yield that is much higher with respect to the flat case is also observed. As can be observed in Fig. 5(a) this happens at a displacement value for of around 7 nm in the flat pillar case, corresponding to about 0.5% strain. For the curved pillar case the strain value at yielding is around 0.8%. This implies a different evaluation of the elastic part of the stress/displacement curve and an underestimation of the elastic modulus. A very similar observation has been already reported for the case of misalignment between a (flat) pillar and the indenter [26]. We recall here that the two simulations start with exactly the same initial dislocation distribution and thus the results should be directly comparable. These differences can be observed for all the considered values for the initial dislocation densities of Fig. 5(a), (b) and (c) but a further analysis can be done looking at Fig. 5(b) and (c), where a much smoother profile can be observed for the case of the flat pillar with stress drops less pronounced with respect to the corresponding case with $h = 10$ nm. Furthermore, the onset of the avalanches is shifted towards much higher strain values in the case of the curved pillars. This is not the case for Fig. 5(a) where the two stress/strain curves show a very similar evolution and stress drops that are almost comparable. In this case dislocation avalanches start early at the same displacement value of around 13 nm, with the two considered stress strain curves following a very similar path, apart from the difference in the elastic regime already discussed.

The avalanches behavior has been further analyzed in Fig. 6(a) where the maximum stress drop recorded $\Delta\sigma_{max}$ is plotted against the dislocation density ρ. As can be seen in the figure, the stress drops observed are quite similar for the lowest dislocation density considered while they start to differ substantially when the dislocation density increases. For the case of the flat pillar the stress drops *decrease* with

increasing dislocation density, while the opposite is true for the case of a pillar with curved top free surface. The very similar behavior at the lowest dislocation density is probably due to the low number of dislocation sources present in the pillar. In this case the presence of an inhomogeneous stress field as in the case of the curved pillar has less impact on the dislocation evolution since only a small number of dislocation sources are present and can be activated. At higher initial dislocation densities, on the contrary, the presence of a strongly inhomogeneous stress field activates a lot of dislocations sources in the top region of the pillar, and the interaction between these ones and the rest of the initial loops will strongly modify the subsequent evolution.

A very similar trend can be observed also in Fig. 6(b). Here, a different statistical measure for the stress drops in the plastic part of the stress/strain curves has been considered: the standard deviation of the stress dishomogeneities ($\Delta\sigma$). Again, the two behaviors for the case of the flat and the curved pillar can be clearly distinguished, with an initial value very similar for the two cases at the lowest dislocation density. The flat pillar then shows a strong decrease of the stress inhomogeneities with respect to the dislocation density. For the curved pillar, on the other hand this trend is less pronounced and the standard deviation of the stress field do not decrease so drastically with respect to the dislocation density and indeed remains quite constant at very high values. Finally, the relative difference in elastic modulus (E) is also reported in the plot of Fig. 6(b) (black triangles). This plot quantifies the underestimation of the elastic constants in the elastic part of the stress–strain curve when performing a compression testing of a non-flat micropillars. In all the cases investigated the difference is quite substantial (as it is clearly observable also from the stress–strain curves of Fig. 5) and corresponds to about $30-35\%$ of the elastic modulus.

All the analysis here reported thus confirm the strong impact of a relatively small isotropic curvature for the free surface geometry on the interpretation of compression experiments. Both the evaluation of the elastic part of the stress–strain curve both the plastic deformation and the evolution of the dislocation microstructure are drastically affected by such a deviation from the ideal geometry. It is worth noticing that the effect of curvature can change principal trends in uniaxial pillar compression size effects, theoretically expected [42–44]. As shown in experimentally benchmarked models [44], the size of stress drops shall increase with decreasing size or equivalently with decreasing dislocation density. Here, we find that a small, isotropic top-surface curvature, may reverse this trend and induce larger stress drops with increasing dislocation density, given that larger dislocation densities make the externally induced stress inhomogeneity to become predominant in the overall mechanics solution. This capability towards such trend reversals in metals at realistic conditions, may be the very cause for common confusions in experimental data interpretations [10].

4. Conclusions

In this Paper, we presented a theoretical investigation of the uniaxial compression of realistic metallic (Cu) micropillars, by means of a coupled FE/DDD approach. In particular, we investigated the effect of a small curvature on the top surface of the micropillar, on the mechanical response of such systems. Large stress inhomogeneities are produced as a result of such small curvatures, as opposed to the uniform stress condition that is basically implied in theoretical studies of uniaxially compressed micropillars [10,41,43]. We showed that this stress concentration strongly influences the evolution of the dislocation microstructure with an appreciable effect also on the stress/displacement curve, that can indeed reverse basic theoretical expectations, such as the decrease of avalanche noise with increasing dislocation density [44]. higher stress drops are observed in the stress/displacement curve with increasing dislocation density, and higher strains at yield are typically recorded for pillars with non-flat top free surface due to a sub-linear elastic part in the elastic regime of the stress/displacement curve.

The results shown in this Paper are thus directed towards a better understanding of a widely exploited experimental procedure used for the uniaxial compression of micropillars. We showed by a computational investigation of these systems that the presence of small surface inhomogeneities at the top free surface can drastically change the expectations of homogeneous applied stresses in the pillar and the subsequent interpretations of stress/displacement curves. Future work needs to focus on characterizing the crossover behavior as curvature is decreased and key signatures that may be identifiable in realistic experimental conditions, for setting criteria and thresholds, for a safer and deeper understanding of the materials science, as opposed to the mechanics behavior, of single-crystal micropillar experiments.

CRediT authorship contribution statement

Fabrizio Rovaris: Conceptualization, Investigation, Methodology, Software, Writing – original draft. **Stefanos Papanikolaou:** Conceptualization, Writing – review & editing, Supervision. **Mikko J. Alava:** Conceptualization, Writing – review & editing, Supervision.

Declaration of competing interest

The authors declare that they have no known competing financial interests or personal relationships that could have appeared to influence the work reported in this paper.

Acknowledgments

We acknowledge support from the European Union Horizon 2020 research and innovation program under grant agreement no. 857470 and from the European Regional Development Fund via the Foundation for Polish Science International Research Agenda PLUS program grant No. MAB PLUS/2018/8. We acknowledge the computational resources provided by the High Performance Cluster at the National Centre for Nuclear Research in Poland.

References

[1] Qiaoyan Sun, Qiang Guo, Xi Yao, Lin Xiao, Julia R. Greer, Jun Sun, Size effects in strength and plasticity of single-crystalline titanium micropillars with prismatic slip orientation, Scr. Mater. 65 (6) (2011) 473–476.
[2] Sharif Shahbeyk, George Z. Voyiadjis, Vahid Habibi, Sarah Hashemi Astaneh, Mohammadreza Yaghoobi, Review of size effects during micropillar compression test: Experiments and atomistic simulations, Crystals 9 (11) (2019).
[3] D. Kiener, P.J. Guruprasad, S.M. Keralavarma, G. Dehm, A.A. Benzerga, Work hardening in micropillar compression: In situ experiments and modeling, Acta Mater. 59 (10) (2011) 3825–3840.
[4] Michael D. Uchic, Paul A. Shade, Dennis M. Dimiduk, Plasticity of micrometer-scale single crystals in compression, Annu. Rev. Mater. Res. 39 (2009) 361–386.
[5] B. Bellón, S. Haouala, J. LLorca, An analysis of the influence of the precipitate type on the mechanical behavior of Al - Cu alloys by means of micropillar compression tests, Acta Mater. 194 (2020) 207–223.
[6] Michael D Uchic, Dennis M Dimiduk, Jeffrey N Florando, William D Nix, Sample dimensions influence strength and crystal plasticity, Science 305 (5686) (2004) 986–989.
[7] Julia R. Greer, Ju Young Kim, Michael J. Burek, The in-situ mechanical testing of nanoscale single-crystalline nanopillars, J. Mecah. 61 (12) (2009) 19–25.
[8] Julia R. Greer, Dongchan Jang, X. Wendy Gu, Exploring deformation mechanisms in nanostructured materials, J. Mecah. 64 (10) (2012) 1241–1252.
[9] Andrew T. Jennings, Ju Li, Julia R. Greer, Emergence of strain-rate sensitivity in Cu nanopillars: Transition from dislocation multiplication to dislocation nucleation, Acta Mater. 59 (14) (2011) 5627–5637.
[10] Stefanos Papanikolaou, Yinan Cui, Nasr Ghoniem, Avalanches and plastic flow in crystal plasticity: an overview, Modelling Simulation Mater. Sci. Eng. 26 (1) (2017) 013001.
[11] Haidong Fan, Qingyuan Wang, Jaafar A. El-Awady, Dierk Raabe, Michael Zaiser, Strain rate dependency of dislocation plasticity, Nature Commun. 12 (1) (2021) 1–11.
[12] Hyung-Jun Chang, Marc Fivel, David Rodney, Marc Verdier, Multiscale modelling of indentation in FCC metals: From atomic to continuum, Compt. Rendus Phys. 11 (3–4) (2010) 285–292.

[13] A.S. Schneider, B.G. Clark, C.P. Frick, P.A. Gruber, E. Arzt, Effect of orientation and loading rate on compression behavior of small-scale mo pillars, Mater. Sci. Eng. A 508 (1–2) (2009) 241–246.
[14] C.P. Frick, B.G. Clark, S. Orso, A.S. Schneider, E. Arzt, Size effect on strength and strain hardening of small-scale [1 1 1] nickel compression pillars, Mater. Sci. Eng. A 489 (1–2) (2008) 319–329.
[15] Caizhi Zhou, Irene J. Beyerlein, Richard Lesar, Plastic deformation mechanisms of fcc single crystals at small scales, Acta Mater. 59 (20) (2011) 7673–7682.
[16] Ill Ryu, Wei Cai, William D. Nix, Huajian Gao, Stochastic behaviors in plastic deformation of face-centered cubic micropillars governed by surface nucleation and truncated source operation, Acta Mater. 95 (2015) 176–183.
[17] Seunghwa Ryu, Keonwook Kang, Wei Cai, Predicting the dislocation nucleation rate as a function of temperature and stress, J. Mater. Res. 26 (18) (2011) 2335–2354.
[18] Oliver Kraft, Patric A Gruber, Reiner Mönig, Daniel Weygand, Plasticity in confined dimensions, Annu. Rev. Mater. Res. 40 (2010) 293–317.
[19] T.H. Sung, J.C. Huang, J.H. Hsu, S.R. Jian, Mechanical response of GaN film and micropillar under nanoindentation and microcompression, Appl. Phys. Lett. 97 (17) (2010) 1–4.
[20] T.H. Sung, J.C. Huang, J.H. Hsu, S.R. Jian, Mechanical response of GaN film and micropillar under nanoindentation and microcompression, Appl. Phys. Lett. 97 (17) (2010) 1–4.
[21] J.M. Wheeler, J. Michler, Elevated temperature, nano-mechanical testing in situ in the scanning electron microscope, Rev. Sci. Instrum. 84 (4) (2013) 1–15.
[22] A.K. Basak, A. Pramanik, C. Prakash, Deformation and strengthening of SiC reinforced Al-MMCs during in-situ micro-pillar compression, Mater. Sci. Eng. A 763 (2019) 138141.
[23] Yang Hu, Li Shu, Qun Yang, Wei Guo, Peter K. Liaw, Karin A. Dahmen, Jian Min Zuo, Dislocation avalanche mechanism in slowly compressed high entropy alloy nanopillars, Commun. Phys. 1 (1) (2018) 1–8.
[24] Yuan Xiao, Roksolana Kozak, Michel J.R. Haché, Walter Steurer, Ralph Spolenak, Jeffrey M. Wheeler, Yu Zou, Micro-compression studies of face-centered cubic and body-centered cubic high-entropy alloys: Size-dependent strength, strain rate sensitivity, and activation volumes, Mater. Sci. Eng. A 790 (2020) 139429.
[25] Karol Frydrych, Kamran Karimi, Michal Pecelerowicz, Rene Alvarez, Francesco Javier Dominguez-Gutiérrez, Fabrizio Rovaris, Stefanos Papanikolaou, Materials informatics for mechanical deformation: A review of applications and challenges, Materials 14 (19) (2021).
[26] H. Zhang, B.E. Schuster, Q. Wei, K.T. Ramesh, The design of accurate micro-compression experiments, Scr. Mater. 54 (2) (2006) 181–186.
[27] Huiyang Fei, Amit Abraham, Nikhilesh Chawla, Hanqing Jiang, Evaluation of micro-pillar compression tests for accurate determination of elastic-plastic constitutive relations, J. Appl. Mech. 79 (6) (2012).
[28] Robert John Amodeo, Nasr Mostafa Ghoniem, Dislocation dynamics. I. A proposed methodology for deformation micromechanics, Phys. Rev. B 41 (10) (1990) 6958.
[29] B. Devincre, L.P. Kubin, Simulations of forest interactions and strain hardening in fcc crystals, Modelling Simulation Mater. Sci. Eng. 2 (3A) (1994) 559.
[30] Ray S. Fertig, Shefford P. Baker, Simulation of dislocations and strength in thin films: A review, Prog. Mater. Sci. 54 (6) (2009) 874–908.
[31] Julia R. Greer, Christopher R. Weinberger, Wei Cai, Comparing the strength of f.c.c. and b.c.c. sub-micrometer pillars: Compression experiments and dislocation dynamics simulations, Mater. Sci. Eng. A 493 (1) (2008) 21–25.
[32] Erik Van der Giessen, Alan Needleman, Discrete dislocation plasticity: a simple planar model, Modelling Simulation Mater. Sci. Eng. 3 (5) (1995) 689.
[33] D. Gomez-Garcia, B. Devincre, L.P. Kubin, Dislocation dynamics in confined geometry, J. Comput.-Aided 6 (1999) 157–164.
[34] Anders Logg, Kent-Andre Mardal, Garth Wells, Automated Solution of Differential Equations By the Finite Element Method, Springer, 2016.
[35] Toshio Mura, Micromechanics of defects in solids, in: S. Nemat-Nasser, G. A.E. Oravas (Eds.), volume 3 ofMechanics of Elastic and Inelastic Solids, second ed., Dordrecht, 1987.
[36] O. Jamond, R. Gatti, A. Roos, B. Devincre, Consistent formulation for the discrete-continuous model: Improving complex dislocation dynamics simulations, Int. J. Plast. 80 (2016) 19–37.
[37] A. Vattré, B. Devincre, F. Feyel, R. Gatti, S. Groh, O. Jamond, A. Roos, Modelling crystal plasticity by 3D dislocation dynamics and the finite element method: The discrete-continuous model revisited, J. Mech. Phys. Solids 63 (1) (2014) 491–505.
[38] Fabrizio Rovaris, Fabio Isa, Riccardo Gatti, Arik Jung, Giovanni Isella, Francesco Montalenti, Hans von Känel, Three-dimensional SiGe/Si heterostructures: Switching the dislocation sign by substrate under-etching, Phys. Rev. Mater. 1 (7) (2017) 073602.
[39] Wei Cai, A. Arsenlis, C. Weinberger, V. Bulatov, A non-singular continuum theory of dislocations, J. Mech. Phys. Solids 54 (3) (2006) 561–587.
[40] J.D. Eshelby, The determination of the elastic field of an ellipsoidal inclusion, and related problems, in: Proceedings of the Royal Society of London a: Mathematical, Physical and Engineering Sciences, Vol. 241, 1957, pp. 376–396.
[41] Stefanos Papanikolaou, Giacomo Po, Λ-Invariant and topological pathways to influence the strength of submicron crystals, Phys. Rev. Lett. 124 (20) (2020) 205502.
[42] Hengxu Song, Stefanos Papanikolaou, From statistical correlations to stochasticity and size effects in sub-micron crystal plasticity, Metals 9 (8) (2019) 835.
[43] Hengxu Song, Dennis Dimiduk, Stefanos Papanikolaou, Universality class of nanocrystal plasticity: localization and self-organization in discrete dislocation dynamics, Phys. Rev. Lett. 122 (17) (2019) 178001.
[44] Stefanos Papanikolaou, Hengxu Song, Erik Van der Giessen, Obstacles and sources in dislocation dynamics: Strengthening and statistics of abrupt plastic events in nanopillar compression, J. Mech. Phys. Solids 102 (2017) 17–29.